Structure of the N-Terminal RNA-Binding Domain of the SARS CoV Nucleocapsid Protein

Qiulong Huang, Liping Yu, Andrew M. Petros, Angelo Gunasekera, Zhihong Liu, Nan Xu, Philip Hajduk, Jamey Mack, Stephen W. Fesik, and Edward T. Olejniczak*

Global Pharmaceutical Discovery Division, Abbott Laboratories, Abbott Park, Illinois 60064

Received December 1, 2003; Revised Manuscript Received March 24, 2004

ABSTRACT: The severe acute respiratory syndrome (SARS) virus belongs to the Coronaviridea family of viruses. Its virion encodes several proteins including a replicase and four structural proteins. Here we describe the three-dimensional structure of the N-terminal domain of the SARS coronavirus (CoV) nucleocapsid protein. The protein consists of a five-stranded β sheet with a folding topology distinct from other RNA-binding proteins. Single-stranded RNAs bind to the protein surface at the junction between a flexible, positively charged β hairpin and the core structure. NMR-based screening was used to identify low molecular weight compounds that bind to this site.

The severe acute respiratory syndrome (SARS)[1] caused by the human coronavirus (CoV) is a potential worldwide health risk (*1*−*4*). CoVs are known to be responsible for virulent respiratory and enteric diseases in animals (*5*). However, until the SARS CoV appeared in late 2002, human CoVs were normally associated with the generally benign affliction, the common cold (*3*). The recently determined sequence data for human SARS CoV indicate that the SARS CoV is not closely related to any previously known human or animal CoV (*6*−*10*). Its viral RNA genome contains five major open reading frames that encode the replicase polyprotein and four structural proteins composed of the S (spike) glycoprotein, the envelope E protein, the membrane glycoprotein M, and the nucleocapsid protein (NP) (*6*, *8*, *9*). Although the three-dimensional structure of the $3CL^{pro}$ proteinase from the CoV has been reported (*11*, *12*), none of the structural proteins from the SARS CoV has been characterized structurally.

The NP is a structural protein whose primary function is to recognize a stretch of RNA that serves as a packaging signal and leads to the formation of the ribonucleoprotein (RNP) complex during assembly (*5*). The formation of the RNP may also be important for maintaining the RNA in an ordered conformation suitable for replication and transcription of the viral genome. The SARS CoV NP[2] has some sequence homology to other CoV NPs, but it exhibits no significant sequence homology to any other proteins. In murine hepatitis CoV, the NP contains two RNA-binding domains that interact with the 3′ RNA, one located in the amino and one in the carboxy terminal region (*13*). These two domains are part of the three conserved regions of the sequence of the CoV NP and are likely to be conserved to retain strain-independent protein function. The strain-specific sequence variations that are present in the different CoV family members are primarily found between these three conserved regions (*13*).

Here we describe the structure of the N-terminal domain of the SARS CoV NP as determined by nuclear magnetic resonance (NMR) spectroscopy. By identifying the residues of the protein whose resonances were perturbed by the addition of RNA, we have also defined how the protein interacts with RNA. These data were used in conjunction with a NMR-based screen to identify low molecular weight compounds that bind to the RNA-binding face of the protein. Finally, the structure of the protein and its RNA binding are compared to other RNA-binding proteins.

MATERIALS AND METHODS

Sample Preparation. Structural studies were conducted using the N-terminal domain of the SARS CoV NP (residues 45−181), Swiss-Prot accession number P59595. A N-terminal histidine tag (MGSSHHHHHHSSGLVPRGSAM) was added to aid in purification. The coding sequence was amplified by PCR with primers encoding 5′- and 3′-restriction sites. The PCR product was digested and ligated into the *Nco* I and *Xho* I sites of the pET21d(+) plasmid (Novagen, Madison, WI), providing the N-terminal His-tagged protein. Constructs were verified by DNA sequencing.

The protein used in the structural studies was expressed in *Escherichia coli* BL21(DE3) grown on M9 media and purified using Ni-NTA affinity chromatography. Uniformly ^{15}N-labeled, uniformly ^{15}N,^{13}C-labeled, and uniformly ^{2}H,^{15}N,^{13}C-labeled samples were prepared with media containing $^{15}NH_4Cl$, $^{15}NH_4Cl$ plus [U-^{13}C]glucose, or $^{15}NH_4Cl$ plus [U-^{13}C]glucose grown in 75% D_2O, respectively. A biosynthetically directed, fractionally ^{13}C-labeled sample was

* To whom correspondence should be addressed: Abbott Laboratories, 100 Abbott Park Rd., R46Y, AP10, Abbott Park, IL 60064-6098. E-mail: edward.olejniczak@abbott.com. Phone: (847) 937-0298. Fax: (847) 938-2478.

[1] Abbreviations: SARS, severe acute respiratory syndrome; CoV, coronavirus; NP, nucleocapsid protein; RNA, ribonucleic acid; RNP, ribonucleoprotein; NMR, nuclear magnetic resonance; NOE, nuclear Overhauser effect; RMSD, root-mean-squared deviation; MW, molecular weight.

[2] The average minimized coordinates for the SARS CoV NP have been deposited within the Protein Data Bank (PDB 1SSK).

10.1021/bi036155b CCC: $27.50
Published on Web 04/28/2004

Table 1: Structural Statistics and RMSDs for 20 Structures of the N-Terminal SARS CoV NP

	$\langle SA \rangle^a$	$\langle \overline{SA} \rangle_r$
RMSD from Experimental Distance Restraints (Å)		
all (1823)	0.015 ± 0.001	0.014
intraresidue (408)	0.007 ± 0.003	0.005
sequential (433)	0.009 ± 0.003	0.009
short range (158)	0.015 ± 0.003	0.015
long range (805)	0.016 ± 0.002	0.014
hydrogen bonds (19)	0.031 ± 0.003	0.032
RMSD from Experimental Torsional Angle Restraints (deg)		
ϕ and ψ angles (49)	0.39 ± 0.06	0.28
CNX Potential Energies (kcal mol^{-1})		
E_{tot}	129.1 ± 7.8	107.7
E_{bond}	6.8 ± 0.6	5.5
E_{ang}	72.2 ± 4.1	62.8
E_{imp}	6.4 ± 0.9	4.8
E_{repel}	22.5 ± 2.3	17.3
E_{NOE}	20.4 ± 3.5	16.9
E_{cdih}	0.8 ± 0.3	0.4

Cartesian Coordinate RMSD (Å)	backbone	all heavy
$\langle SA \rangle$ versus $\langle \overline{SA} \rangle^b$	1.15 ± 0.43	1.52 ± 0.38
$\langle SA \rangle$ versus $\langle \overline{SA} \rangle^c$	0.64 ± 0.06	1.09 ± 0.08

ProCheck (*30*) Ramachandran Analysis of $\langle \overline{SA} \rangle_r{}^b$	
residues in the most favored and allowed regions	90.9%
residues in generously allowed regions	9.1%
residues in disallowed regions	0.0%

[a] $\langle SA \rangle$ is the ensemble of the 20 lowest-enegy structures, $\langle \overline{SA} \rangle$ is the mean structure, and $\langle \overline{SA} \rangle_r$ is the energy-minimized mean structure. [b] For residues 49−176. [c] Excluding residues 91−106.

also grown using an approach described earlier (*14*). NMR samples contained 0.5−1.0 mM protein in either 90% H_2O/10% ^2H_2O or 100% ^2H_2O containing 50 mM sodium phosphate (pH 6.8) and 100 mM sodium chloride. RNA samples were obtained from Operon and used without further purification.

NMR Spectroscopy. All NMR data were acquired at 298 K on a Bruker DRX500, DRX600, or DRX800 NMR spectrometer. Backbone ^1H, ^{13}C, and ^{15}N resonances were assigned using triple-resonance experiments (HNCA, HN(CO)CA, HN(CA)CB, HN(COCA)CB, HNCO, and HN(CA)CO) (*15*). The side-chain ^1H and ^{13}C NMR signals were assigned from 3D HCCH−TOCSY (total correlation spectroscopy), 3D H(CCO)NH−TOCSY, 3D HC(CO)NH−TOCSY, and ^{15}N-edited TOCSY experiments (*16*). Nuclear Overhauser effect (NOE) distance restraints were obtained from 3D ^{15}N- and ^{13}C-edited nuclear Overhauser effect spectroscopy spectra acquired with a mixing time of 80 or 150 ms (*17*, *18*). A $^{15}N/^1HN$ or $^{13}C/^1H$ heteronuclear single quantum coherence spectrum was used in the titration studies to monitor RNA or compound binding. RNA titrations were done with a protein concentration of 50 uM and protein/RNA ratios of 3:1 and 1:1. For compound binding, a total of 8340 low molecular weight compounds were screened in mixtures of 10 at concentrations of 0.5 mM each.

Structure Calculations. SARS CoV NP structures were calculated using a simulated annealing protocol with CNX (Accelrys, San Diego, CA) (*19*). A square-well potential (F_{NOE} = 50 kcal mol^{-1}) was employed to constrain NOE-derived distances. On the basis of the cross-peak intensities, NOE-derived distance restraints were given upper bounds of 3.0, 4.0, 5.0, or 6.0 Å. Torsion angle restraints were generated from an analysis of N, C′, C^α, and H^α chemical shifts using TALOS (*20*). A force constant of 200 kcal mol^{-1} rad^{-2} was applied to all torsional restraints. Explicit hydrogen bonds were included in the β sheets for residues observed to have slowly exchanging amide protons, backbone chemical shifts consistent with a β-sheet secondary structure, and appropriate short-range NOEs (*21*).

RESULTS AND DISCUSSION

The N-terminal domain of the SARS CoV NP (residues 45−181) was cloned and expressed in *E. coli*. Shorter constructs truncated at the N or C terminus were found to be unfolded in solution. The 3D structure of the N-terminal domain of the SARS CoV NP (residues 45−181) was determined using NMR spectroscopy. The resonances were assigned using a suite of triple-resonance experiments on uniformly ^{15}N-, ^{15}N- and ^{13}C-, and ^2H,^{15}N- and ^{13}C-labeled protein samples. The structure was determined from 1804 NOE-derived distance restraints, 19 hydrogen bond restraints derived from an analysis of amide exchange rates, and 49 torsional restraints from an analysis of the backbone chemical shifts (Table 1).

Figure 1 depicts a stereoview of the backbone superposition of 20 low-energy structures of the N-terminal domain of the SARS CoV NP. The structure of the backbone is well-defined by the NMR data except for the extended β hairpin ($\beta2'$, $\beta3'$). This region has significantly smaller heteronuclear $^{15}N\{^1H\}$ NOEs, indicating that the β hairpin is very flexible in solution (Figure 2). The internal hydrophobic residues of the protein (W53, F54, L57, L65, F67, Y88, W109, F111, W133, L160, L162, and F172) are all well-defined by the NMR data. The atomic root-mean-squared deviation (RMSD) for residues 49−176 is 1.15 ± 0.43 Å for the backbone atoms and 1.52 ± 0.38 Å for all heavy atoms. Excluding the residues in the flexible extended β hairpin ($\beta2'$, $\beta3'$, residues

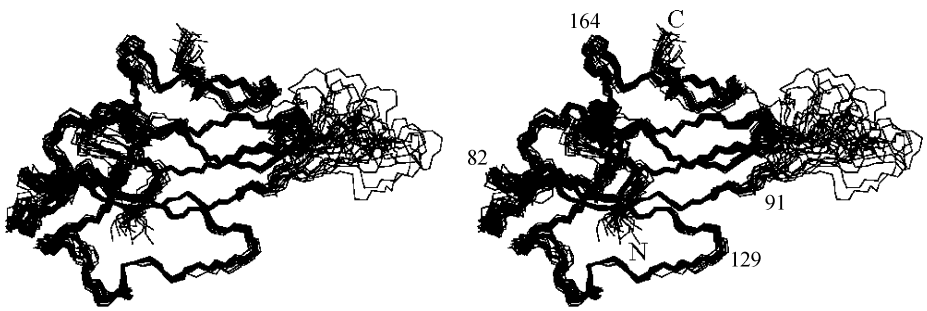

FIGURE 1: Stereoview of the backbone (N,C^α,C′) superposition of 20 low-energy NMR-derived structures for the N-terminal RNA-binding domain of the NP from SARS (residues 49−178). The extended β hairpin is located on the right-hand side of the molecule.

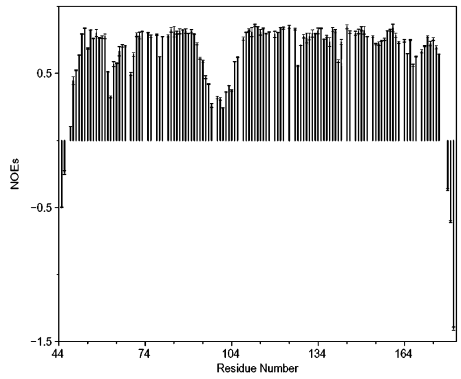

FIGURE 2: Plot of the measured heteronuclear $^{15}N\{^{1}H\}$ NOEs of the backbone amides and their uncertainties as a function of the residue number. The residues for which no results are shown correspond to 11 prolines and the residues for which the backbone amide assignments could not be obtained.

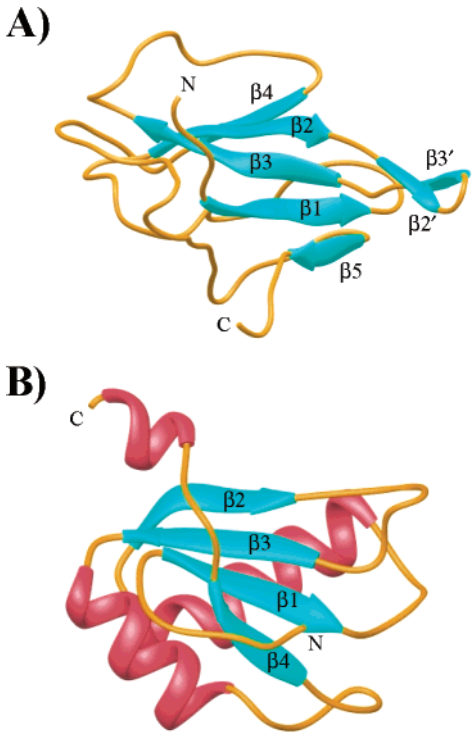

FIGURE 3: (A) Ribbons (*31*) representation of the RNA-binding domain of the N-terminal domain of the NP from SARS (residues 49−178). (B) Ribbons plot showing the U1A RNA-binding protein (PDB 1URN) (*26*).

91−106), the backbone RMSD is reduced to 0.64 ± 0.06 Å for the backbone atoms and 1.09 ± 0.08 Å for all heavy atoms. The structural statistics for the ensemble and energy-minimized structure are given in Table 1.

The structure of the protein consists of a five-stranded antiparallel β sheet with the topology $\beta4-\beta2-\beta3-\beta1-\beta5$ (Figure 3A). The first strand ($\beta1$) is located near the N terminus and is followed by a long loop to $\beta2$. $\beta2$ is connected to $\beta3$ via a β hairpin ($\beta2'-\beta3'$) that extends beyond the core of the protein. The residues in the extended β hairpin are predominantly basic with 5 of the 15 residues being arginines or lysines. A loop located above the β sheet connects $\beta3$ to $\beta4$. $\beta4$ runs antiparallel to $\beta2$ and is connected by another loop that lies below the β sheet to $\beta5$, which runs antiparallel to $\beta1$. The placement of loops on both faces of the β sheet is a distinctive feature of the topology of the protein. The central strand of the β sheet, $\beta3$, contains the highly conserved sequence RWYFYYLGT, which is found in the reported CoV NPs (*6*, *8*, *9*).

A 3D structural homology search with DALI (*22*) found no structure with a *Z* score greater than 1.5, indicating that the N-terminal domain of the SARS CoV NP has very little structural homology to any other protein in the database. Even though the overall fold is very different from any known protein, the N-terminal domain of the SARS CoV NP has some similarities to the RNP-binding motif (*23*−*25*). In particular, neglecting $\beta4$, the β strands of the SARS CoV NP β sheet are analogous to the β strands of an RNP protein (Figure 3B). In addition, the SARS CoV NP as well as the other β-sheet RNA-binding folds all have an exposed loop ($\beta2'-\beta3'$) that extends from two β strands (*24*). In the RNP (*23*, *25*, *26*) and oligonucleotide/oligosaccharide (OB) (*27*) RNA complexes, this loop is used to clamp RNA against the β sheet of the protein. Thus, despite the low sequence and structural homology to known RNA-binding proteins, the SARS CoV NP contains unique structural features consistent with its role in binding RNA.

The ability of the SARS CoV NP to bind RNA was investigated by the addition of several viral 3′ untranslated sequence RNAs. Both a 16mer RNA (AUAUGGAAGAGCCCUA) and a 32mer RNA (CGAGGCCACGCGGAGUACGAUCGAGGGUACAG) showed similar residue-specific shifts or broadening around the junction between the long flexible β hairpin and the core of the protein (Figure 4A). The broadening is most likely due to chemical exchange, which is a result of these residues contacting RNA (*28*). The longer 32mer viral RNA exhibited a greater degree of broadening of the resonances from residues of the protein in this region. Interestingly, addition of a 15mer polyadenine nucleotide still showed some small perturbations. This RNA-binding site of the SARS CoV NP is consistent with the localization of a high concentration of positively charged lysine and arginine residues on its surface (Figure 4B). The long flexible β hairpin with its positively charged surface may grasp RNA against the β sheet similar to what was found for the U1A RNP RNA-binding protein, where a highly positively charged loop between $\beta2$ and $\beta3$ and the face of the β sheet is involved in RNA binding (*25*, *26*).

Using an NMR-based screen (*29*), we have identified several small molecules that bind to the N-terminal domain of the SARS CoV NP. For example, 6-amino-4-hydroxy-naphthalene-2-sulfonic acid is a low molecular weight (MW = 239), low affinity ($K_d \sim 1$ mM) ligand for the SARS CoV NP that binds to the same face of the protein as RNA (Figure 4C). Intriguingly, this compound contains a sulfonate group, which may mimic the phosphate backbone of RNA and interact with the arginines and/or lysines in this region. These compounds may serve as leads for obtaining high-affinity ligands that bind tightly to the protein and impair its function.

CONCLUSIONS

In this paper, we describe the three-dimensional structure of the N-terminal domain of the SARS CoV NP. The protein represents another folding topology that can recognize RNA. The structural elements that the protein uses to recognize RNA are similar to those used by the RNP RNA-binding proteins. We have also identified a low molecular weight

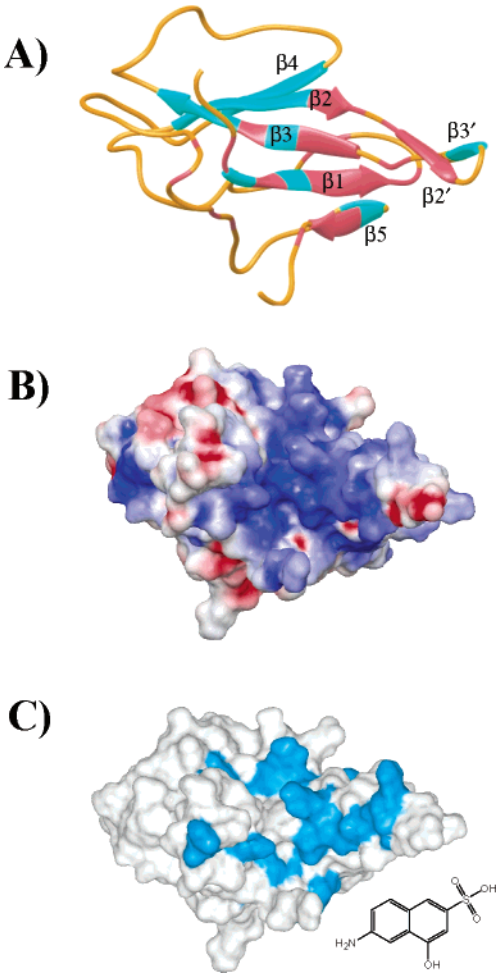

FIGURE 4: (A) Ribbons (*31*) plot of the N-terminal SARS NP illustrating the RNA-binding site (residues 49−178). The ribbon is colored red for the residues whose ^{13}C or ^{15}N resonances are perturbed by RNA binding (32mer). (B) Molecular surface of the SARS NP (residues 49−178) prepared with Del Phi (*32*, *33*) colored by local electrostatic potential. Electronegative regions are in red, while electropositive regions are in blue. (C) Surface representation of the N-terminal SARS NP illustrating the binding site for a small molecule lead identified from an NMR-based screen (inset). The orientation is the same as that shown in A and B. The surface is colored blue for residues whose ^{15}N resonances are perturbed upon binding of the ligand.

compound that binds to the same face of the protein as RNA. These data may be useful in developing new strategies to treat this human pathogen as well as the animal diseases caused by related CoVs.

REFERENCES

1. Booth, C. M. (2003) Clinical features and short-term outcomes of 144 patients with SARS in the greater Toronto area, *J. Am. Med. Assoc. 289*, 2801−2809.
2. Enserink, M., and Vogel, G. (2003) Infectious diseases−Hungry for details, scientists zoom in on SARS genomes, *Science 300*, 715−717.
3. Holmes, K. V. (2003) SARS coronavirus: a new challenge for prevention and therapy, *J. Clin. Invest. 111*, 1605−1609.
4. Normile, D. (2003) Infectious diseases−Battling SARS on the frontlines, *Science 300*, 714−715.
5. Lai, M. M., and Cavanagh, D. (1997) The molecular biology of coronaviruses, *Adv. Virus Res. 48*, 1−100.
6. Marra, M. A., Jones, S. J. M., Astell, C. R., Holt, R. A., Brooks-Wilson, A., Butterfield, Y. S. N., Khattra, J., Asano, J. K., Barber, S. A., Chan, S. Y., Cloutier, A., Coughlin, S. M., Freeman, D., Girn, N., Griffin, O. L., Leach, S. R., Mayo, M., McDonald, H., Montgomery, S. B., Pandoh, P. K., Petrescu, A. S., Robertson, A. G., Schein, J. E., Siddiqui, A., Smailus, D. E., et al. (2003) The genome sequence of the SARS-associated coronavirus, *Science 300*, 1399−1404.
7. Qin, E., Zhu, Q. Y., Yu, M., Fan, B. C., Chang, G. H., Si, B. Y., Yang, B. A., Peng, W. M., Jiang, T., Liu, B. H., Deng, Y. Q., Liu, H., Zhang, Y., Wang, C., Li, Y. Q., Gan, Y. H., Li, X. Y., Lu, F. S., Tan, G., Cao, W. C., Yang, R. F., Wang, J., Li, W., Xu, Z. Y., Li, Y., Wu, Q. F., Lin, W., Chen, W. J., Tang, L., Deng, Y. F., Han, Y. J., Li, C. F., Lei, M., Li, G. Q., Li, W. J., Lu, H., Shi, J. P., Tong, Z. Z., Zhang, F., Li, S. G., Liu, B., Liu, S. Q., Dong, W., Wong, G. K. S., Yu, J., and Yang, H. M. (2003) A complete sequence and comparative analysis of a SARS-associated virus (Isolate BJ01), *Chin. Sci. Bull. 48*, 941−948.
8. Rota, P. A., Oberste, M. S., Monroe, S. S., Nix, W. A., Campagnoli, R., Icenogle, J. P., Penaranda, S., Bankamp, B., Maher, K., Chen, M. H., Tong, S. X., Tamin, A., Lowe, L., Frace, M., DeRisi, J. L., Chen, Q., Wang, D., Erdman, D. D., Peret, T. C. T., Burns, C., Ksiazek, T. G., Rollin, P. E., Sanchez, A., Liffick, S., Holloway, B., et al. (2003) Characterization of a novel coronavirus associated with severe acute respiratory syndrome, *Science 300*, 1394−1399.
9. Ruan, Y. J., Wei, C. L., and Ling, A. E. (2003) Comparative full-length genome sequence analysis of 14 SARS coronavirus isolates and common mutations associated with putative origins of infection, *Lancet 361*, 1779−1785.
10. Zeng, F. Y., Chan, C. W. M., Chan, M. N., Chen, J. D., Chow, K. Y. C., Hon, C. C., Hui, K. H., Li, J., Li, V. Y. Y., Wang, C. Y., Wang, P. Y., Guan, Y., Zheng, B., Poon, L. L. M., Chan, K. H., Yuen, K. Y., Peiris, J. S. M., and Leung, F. C. (2003) The complete genome sequence of severe acute respiratory syndrome coronavirus strain HKU-39849 (HK-39), *Exp. Biol. Med. 228*, 866−873.
11. Anand, K., Ziebuhr, J., Wadhwani, P., Mesters, J. R., and Hilgenfeld, R. (2003) Coronavirus main proteinase (3CL(pro)) structure: Basis for design of anti-SARS drugs, *Science 300*, 1763−1767.
12. Yang, H. T., Yang, M. J., Ding, Y., Liu, Y. W., Lou, Z. Y., Zhou, Z., Sun, L., Mo, L. J., Ye, S., Pang, H., Gao, G. F., Anand, K., Bartlam, M., Hilgenfeld, R., and Rao, Z. H. (2003) The crystal structures of severe acute respiratory syndrome virus main protease and its complex with an inhibitor, *Proc. Natl. Acad. Sci. U.S.A. 100*, 13190−13195.
13. Nelson, G. W., Stohlman, S. A., and Tahara, S. M. (2000) High affinity interaction between nucleocapsid protein and leader/intergenic sequence of mouse hepatitis virus RNA, *J. Gen. Virol. 81*, 181−188.
14. Neri, D., Szyperski, T., Otting, G., Senn, H., and Wuthrich, K. (1989) Stereospecific nuclear magnetic resonance assignments of the methyl groups of valine and leucine in the DNA-binding domain of the 434 repressor by biosynthetically directed fractional 13C labeling, *Biochemistry 28*, 7510−7516.
15. Yamazaki, T., Tochio, H., Furui, J., Aimoto, S., and Kyogoku, Y. (1997) Assignment of backbone resonances for larger proteins using the ^{13}C-^{1}H coherence of a $^{1}H^{\alpha}$, ^{2}H, ^{13}C, and ^{15}N-labeled sample, *J. Am. Chem. Soc. 119*, 872−880.
16. Clore, G. M., and Gronenborn, A. M. (1998) NMR Structure Determination of Proteins and Protein complexes larger than 20 kDa, *Curr. Opin. Chem. Biol. 2*, 564−570.
17. Fesik, S. W., and Zuiderweg, E. R. P. (1988) Heteronuclear three-dimensional NMR spectroscopy. A strategy for the simplification of homonuclear two-dimansional NMR spectra, *J. Magn. Reson. 78*, 588−593.
18. Ikura, M., Kay, L. E., Tschudin, R., and Bax, A. (1990) Three-dimensional NOESY−HMQC spectroscopy of a ^{13}C-labeled protein, *J. Magn. Reson. 86*, 204−209.
19. Brunger, A. T. (1992) *X-PLOR, Version 3.1 A System for X-ray Crystallography and NMR*, Yale University Press, New Haven, CT.
20. Cornilescu, G., Delaglio, F., and Bax, A. (1999) Protein backbone angle restraints from searching a database for chemical shift and sequence homology, *J. Biomol. NMR 13*, 289−302.
21. Wuthrich, K. (1986) *NMR of Proteins and Nucleic Acids*, John Wiley & Sons, Inc., New York, NY.
22. Holm, L., and Sander, C. (1993) Protein structure comparison by alignment of distance matrices, *J. Mol. Biol. 233*, 123−138.
23. Ding, J. Z., Hayashi, M. K., Zhang, Y., Manche, L., Krainer, A. R., and Xu, R. M. (1999) Crystal structure of the two-RRM

domain of hnRNP A1 (UP1) complexed with single-stranded telomeric DNA, *Genes Dev. 13*, 1102−1115.
24. Draper, D. E. (1999) Themes in RNA-protein recognition, *J. Mol. Biol. 293*, 255−270.
25. Nagai, K., Oubridge, C., Ito, N., Avis, J., and Evans, P. (1995) The RNP domain: a sequence-specific RNA-binding domain involved in processing and transport of RNA, *Trends Biochem. Sci. 20*, 235−240.
26. Oubridge, C., Ito, N., Evans, P. R., Teo, C. H., and Nagai, K. (1994) Crystal structure at 1.92-Å resolution of the RNA-binding domain of the U1A spliceosomal protein complexed with an RNA hairpin, *Nature 372*, 432−438.
27. Bogden, C. E., Fass, D., Bergman, N., Nichols, M. D., and Berger, J. M. (1999) The structural basis for terminator recognition by the Rho transcription termination factor, *Mol. Cell 3*, 487−493.
28. Matsuo, H., Walters, K. J., Teruya, K., Tanaka, T., Gassner, G. T., Lippard, S. J., Kyogoku, Y., and Wagner, G. (1999) Identification by NMR spectroscopy of residues at contact surfaces in large, slowly exchanging macromolecular complexes, *J. Am. Chem. Soc. 121*, 9903−9904.
29. Shuker, S. B., Hajduk, P. J., Meadows, R. P., and Fesik, S. W. (1996) Discovering high-affinity ligands for proteins: SAR by NMR, *Science 274*, 1531−1534.
30. Laskowski, R. A., Rullmann, J. A., MacArthur, M. W., Kaptein, R., and Thornton, J. M. (1996) Procheck-NMR: Programs for checking the quality of protein structures by NMR, *J. Biomol. NMR 8*, 477−486.
31. Carson, M. (1987) A Ribbons Representation of Macromolecules, *J. Mol. Graphics 5*, 103−106.
32. Honig, B., and Nicholls, A. (1995) Classical electrostatics in biology and chemistry, *Science 268*, 1144−1149.
33. Nichols, A. J., Sharp, K. A., and Honig, B. (1991) Protein folding and association: Insights from interfacial and thermodynamic properties of hydrocarbons, *Proteins: Struct., Funct., Genet. 11*, 281−296.

BI036155B